

Attila Szucs, Robert C. Elson, Michail I. Rabinovich, Henry D. I. Abarbanel and Allen I. Selverston

J Neurophysiol 85:1623-1638, 2001.

You might find this additional information useful...

This article cites 43 articles, 18 of which you can access free at:

<http://jn.physiology.org/cgi/content/full/85/4/1623#BIBL>

This article has been cited by 5 other HighWire hosted articles:

Analysis and Simulation of Gain Control and Precision in Crayfish Visual Interneurons

R. M. Glantz and J. P. Schroeter

J Neurophysiol, November 1, 2004; 92 (5): 2747-2761.

[\[Abstract\]](#) [\[Full Text\]](#) [\[PDF\]](#)

Motor-Unit Coherence During Isometric Contractions Is Greater in a Hand Muscle of Older Adults

J. G. Semmler, K. W. Kornatz and R. M. Enoka

J Neurophysiol, August 1, 2003; 90 (2): 1346-1349.

[\[Abstract\]](#) [\[Full Text\]](#) [\[PDF\]](#)

Amplitude and Frequency Dependence of Spike Timing: Implications for Dynamic Regulation

J. D. Hunter and J. G. Milton

J Neurophysiol, July 1, 2003; 90 (1): 387-394.

[\[Abstract\]](#) [\[Full Text\]](#) [\[PDF\]](#)

Synaptic Modulation of the Interspike Interval Signatures of Bursting Pyloric Neurons

A. Szucs, R. D. Pinto, M. I. Rabinovich, H. D. I. Abarbanel and A. I. Selverston

J Neurophysiol, March 1, 2003; 89 (3): 1363-1377.

[\[Abstract\]](#) [\[Full Text\]](#) [\[PDF\]](#)

Inhibitory Synchronization of Bursting in Biological Neurons: Dependence on Synaptic Time Constant

R. C. Elson, A. I. Selverston, H. D. I. Abarbanel and M. I. Rabinovich

J Neurophysiol, September 1, 2002; 88 (3): 1166-1176.

[\[Abstract\]](#) [\[Full Text\]](#) [\[PDF\]](#)

Medline items on this article's topics can be found at <http://highwire.stanford.edu/lists/artbytopic.dtl> on the following topics:

Physiology .. Membrane Potential

Physiology .. Interneurons

Physiology .. Motor Neurons

Medicine .. Pacemaker

Updated information and services including high-resolution figures, can be found at:

<http://jn.physiology.org/cgi/content/full/85/4/1623>

Additional material and information about *Journal of Neurophysiology* can be found at:

<http://www.the-aps.org/publications/jn>

This information is current as of November 10, 2009 .

Nonlinear Behavior of Sinusoidally Forced Pyloric Pacemaker Neurons

ATTILA SZŰCS,^{1,3} ROBERT C. ELSON,¹ MICHAIL I. RABINOVICH,¹ HENRY D. I. ABARBANEL,^{1,2} AND ALLEN I. SELVERSTON¹

¹Institute for Nonlinear Science, ²Department of Physics, and Marine Physical Laboratory, Scripps Institution of Oceanography, University of California, San Diego, California 92093-0402; and ³Balaton Limnological Research Institute of the Hungarian Academy of Sciences, H-8237 Tihany, Hungary

Received 24 May 2000; accepted in final form 18 December 2000

Szűcs, Attila, Robert C. Elson, Michail I. Rabinovich, Henry D. I. Abarbanel, and Allen I. Selverston. Nonlinear behavior of sinusoidally forced pyloric pacemaker neurons. *J Neurophysiol* 85: 1623–1638, 2001. Periodic current forcing was used to investigate the intrinsic dynamics of a small group of electrically coupled neurons in the pyloric central pattern generator (CPG) of the lobster. This group contains three neurons, namely the two pyloric dilator (PD) motoneurons and the anterior burster (AB) interneuron. Intracellular current injection, using sinusoidal waveforms of varying amplitude and frequency, was applied in three configurations of the pacemaker neurons: 1) the complete pacemaker group, 2) the two PDs without the AB, and 3) the AB neuron isolated from the PDs. Depending on the frequency and amplitude of the injected current, the intact pacemaker group exhibited a wide variety of nonlinear behaviors, including synchronization to the forcing, quasiperiodicity, and complex dynamics. In contrast, a single, broad 1:1 entrainment zone characterized the response of the PD neurons when isolated from the main pacemaker neuron AB. The isolated AB responded to periodic forcing in a manner similar to the complete pacemaker group, but with wider zones of synchronization. We have built an analog electronic circuit as an implementation of a modified Hindmarsh-Rose model for simulating the membrane potential activity of pyloric neurons. We subjected this electronic model neuron to the same periodic forcing as used in the biological experiments. This four-dimensional electronic model neuron reproduced the autonomous oscillatory firing patterns of biological pyloric pacemaker neurons, and it expressed the same stationary nonlinear responses to periodic forcing as its biological counterparts. This adds to our confidence in the model. These results strongly support the idea that the intact pyloric pacemaker group acts as a uniform low-dimensional deterministic nonlinear oscillator, and the regular pyloric oscillation is the outcome of cooperative behavior of strongly coupled neurons, having different dynamical and biophysical properties when isolated.

INTRODUCTION

The voltage behavior of bursting neurons typically arises from the interplay of many ionic currents, synaptic and intracellular processes (Calabrese 1998; Canavier et al. 1991; Stein et al. 1997). The neurons can cooperate to generate coordinated, synchronized activity as a result of their synaptic coupling or in response to external driving inputs. To investigate these properties further, we have studied the responses to sinusoidal current injection of a small circuit of motor pattern generating neurons, both as individuals and as an electrically

coupled group. Using linear and nonlinear analytical techniques, we uncovered rich dynamical behavior that was not analyzed in previous studies of entrainment (Ayers and Selverston 1979).

Periodic stimulation of nonlinear biological and physical systems offers a natural method for investigating their intrinsic dynamics. Stimulation by sinusoidal waveforms of the form $A \sin(2\pi ft)$ with different amplitudes A and frequencies f can drive the system into a wide repertoire of responses including periodic or chaotic temporal patterns (Tomita 1986). Periodic current injection has been used to map the dynamical behavior of squid giant axons (Aihara 1984; Kaplan et al. 1996), snail neurons (Chillemi et al. 1997), and embryonic chick heart cells (Glass et al. 1986), as well as mathematical models of neurons (Matsugu et al. 1998; Wang et al. 2000). Frequency- and intensity-dependent responses characteristic of deterministic nonlinear oscillators have been demonstrated in these experiments and models. Periodic stimulation of nerve fibers or single neurons has also proven to be an effective tool for examining the information processing strategies of the nervous system at cellular level (Hooper 1998; Segundo et al. 1998). Strong evidence of chaotic activity has been found in hippocampal CA3 neurons receiving periodic inputs via mossy fiber stimulation (Hayashi and Ishizuka 1995). This indicates deterministic dynamical behavior in complex multicomponent neural assemblies.

Previous work on sinusoidal stimulation of biological neural networks has focused either on single neurons or very large populations of interconnected neurons. In this paper we examine the response to periodic forcing of a small subset of the very well characterized pyloric central pattern generator (CPG) network of lobster. Our experimental preparation, the pyloric CPG in the stomatogastric ganglion (STG) of the lobster, has served as an experimental model of cellular plasticity and dynamic network organization (Harris-Warrick et al. 1992; Marder 1997; Selverston and Moulins 1987). The STG contains three electrically coupled neurons that form the pacemaker group of the pyloric CPG. These neurons [the anterior burster (AB) and 2 pyloric dilators (PD)] receive inhibitory chemical synapses from other pyloric motor neurons and generate a regular oscillatory pattern with a cycle period of ≈ 1 s. The ventricular dilator neuron (VD) is weakly connected to the

Address for reprint requests: A. Szűcs, Institute for Nonlinear Science, University of California, San Diego, CA 92093-0402 (E-mail: aszucs@ucsd.edu).

The costs of publication of this article were defrayed in part by the payment of page charges. The article must therefore be hereby marked "advertisement" in accordance with 18 U.S.C. Section 1734 solely to indicate this fact.

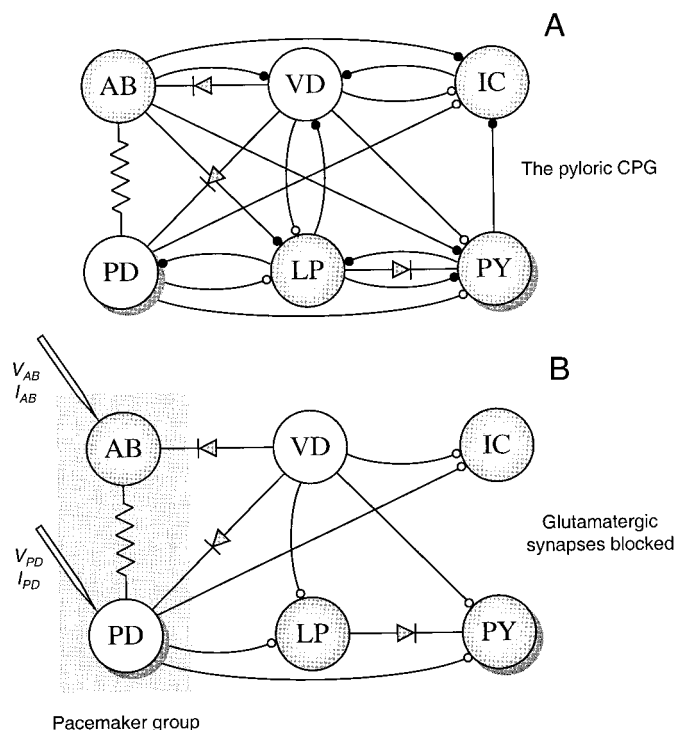


FIG. 1. Circuit diagram of pyloric central pattern generator (CPG; A) and partial isolation of the pacemaker group with picrotoxin (PTX; B). PTX blocks fast glutamatergic synapses (●) while not affecting cholinergic ones (○). There are further modulatory inputs arriving from the gastric CPG and anterior ganglia not shown here. The pacemaker group AB/PD(2) is highlighted. We forced the neurons of the pacemaker group with $I_{\sin}(t) = A \sin(2\pi ft)$. Simultaneously, we measured the membrane potentials of the cells, V_{AB} and V_{PD} , respectively. AB, anterior burster; VD, ventricular dilator; IC, inferior cardiac; PD, pyloric dilator; LP, lateral pyloric; PY, pyloric.

PD and AB neurons by a rectifying electrotonic synapse (Johnson et al. 1993), but it is not commonly considered as part of the pacemaker group. We show in Fig. 1 the circuit layout for the pyloric CPG with the pacemaker group highlighted. The pyloric neurons also receive tonic neuromodulatory inputs from anterior centers of the stomatogastric nervous system.

Using pharmacological tools, one can isolate the pyloric pacemaker group from fast synaptic inputs coming from other pyloric neurons (Fig. 1B). This small functional group of neurons still produces the main pyloric rhythm, often more regular than in intact preparations. This rhythm, however, can be observed only if neuromodulatory inputs from anterior ganglia are left intact (Bal et al. 1988). Besides the pyloric CPG, the stomatogastric nervous system contains other motor pattern generating networks, which typically run at a lower frequency. The interaction of the pyloric circuit with the gastric network has already been studied (Bartos and Nusbaum 1997; Clemens et al. 1998). The periodic forcing of the pacemaker neurons at low frequencies offers a way to simulate, in some respects, the effects of this intercircuit interaction.

The periodic forcing of oscillators is a familiar topic in physical systems. The behavior of such oscillators is described in the parameter plane with coordinates (A, f) (amplitude and frequency of the forcing) (Glass and Mackey 1988). In this plane different regions of synchronization form domains narrowing to a point on the $A = 0$ axis; these regions are known as "Arnol'd tongues." In our experiments the overall oscillator

is a composite of several nonlinear, complex oscillators; however, the pacemaker group displays zones of synchronization and Arnol'd tongues at frequencies near the harmonics and subharmonics of the intrinsic pyloric frequency.

In addition to neurophysiological experiments, we performed sinusoidal forcing experiments with an analog electronic implementation of the modified Hindmarsh-Rose model of bursting neurons (Hindmarsh and Rose 1984; Pinto et al. 2000). The electronic model neuron (EN) was based on nonlinear analysis of membrane voltage time series, which show that only three to five degrees of freedom are operating in the membrane voltage activity of the pacemaker neurons. We have compared the EN's response to periodic current forcing with that in living neurons, and we show them to be substantially the same.

METHODS

We performed experiments on adult intermolt California spiny lobsters *Panulirus interruptus*. The animals were obtained from a local fisherman and kept in large tanks of running, aerated seawater.

Preparation

The preparation has been described previously (Mulloney and Selverston 1974). Briefly, the complete stomatogastric nervous system containing the STG, the esophageal ganglion (OG), and the two commissural ganglia (COG) was separated from the stomach and pinned in a silicone elastomer (Sylgard)-lined Petri dish. Dissection was performed in *Panulirus* physiological saline containing (in mM/l) 483 NaCl, 12.7 KCl, 13.7 CaCl₂, 10 MgSO₄, 4 NaSO₄, 5 HEPES, and 5 TES; pH was set to 7.40. The STG was desheathed using sharp forceps to facilitate access to the somata of the cells. The stomatogastric ganglion was enclosed in a small petroleum jelly (Vaseline) well for separate perfusion. The STG was superfused with saline containing 7.5 μ M picrotoxin (PTX) for a minimum of 30 min. This treatment effectively blocked glutamatergic synaptic inputs to the cells resulting in near complete pharmacological isolation of the pyloric pacemaker group (Bidaut 1980; Marder and Eisen 1984) (Fig. 1B). Anterior centers of the nervous system (COGs, OG, and interconnecting nerves) were always bathed in normal saline. The temperature of the bathing solution was held at 16–18°C using a thermoelectric Peltier-device attached to the bottom surface of the preparation chamber. Reduced configurations of the pacemaker group were obtained by photoinactivating selected neurons by filling them with 5,6-carboxyfluorescein and exposing them to bright blue light (Selverston and Miller 1980).

Electrophysiology

Membrane potentials of the neurons were recorded using glass microelectrodes of 10–15 M Ω filled with 3 M K-acetate plus 0.1 M KCl solution. Membrane potentials of the cells were measured with Neuroprobe 1600 current-clamp amplifiers (AM-Systems). Sinusoidal current command signals were generated either by a Tektronix CFG250 waveform generator or by computer running LabView 5.0 software and equipped with a National Instruments PCI-MIO-16E4 AD/DA converter. The amplitude of the sinusoidal current was between 0.5 and 2.5 nA, while the frequency ranged from 0.2 to 4.0 Hz. The current was injected into one of the neurons while recording from both the injected cell and the cells coupled to it. The extra- and intracellular signals were acquired at a 5- to 10-kS/s rate using the Axoscope 7 program (Axon Instruments) running on a Pentium-266 computer.

Care was taken to monitor the stationarity of the intrinsic pyloric

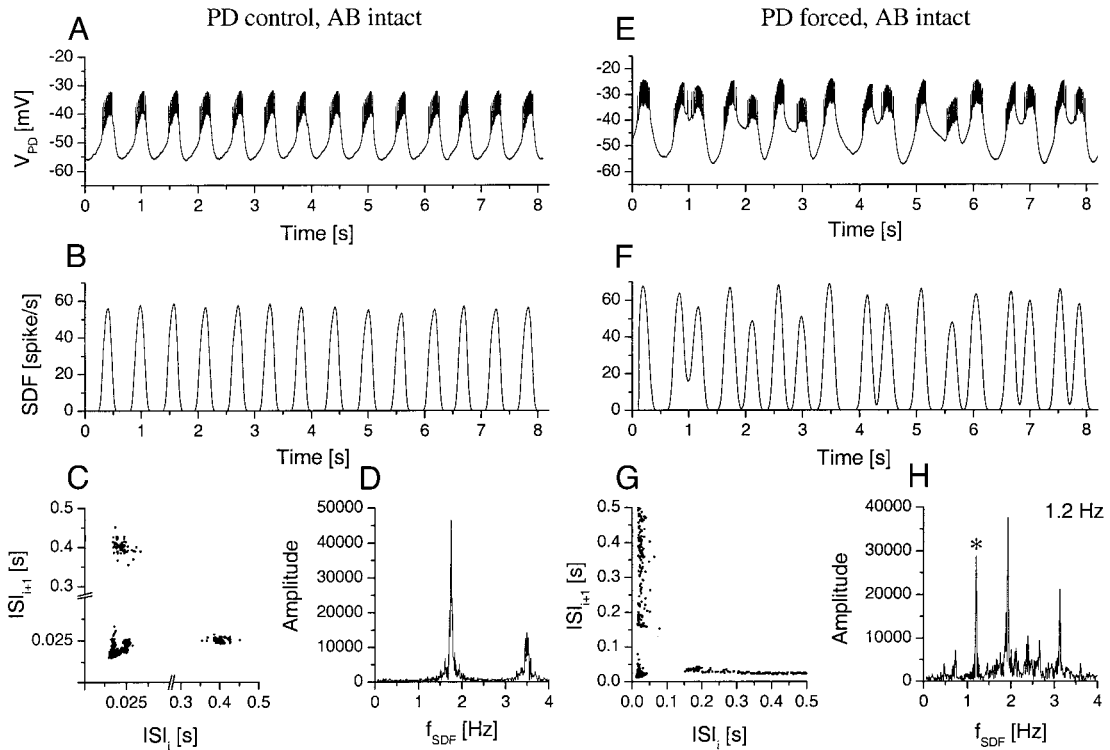


FIG. 2. PD neurons in intact pacemaker group express regular oscillatory firing patterns, and they are able to maintain the pyloric oscillation during periodic forcing. *A*: membrane potential of the PD neuron in intact pacemaker group ($7.5 \mu\text{M}$ PTX in bath). *B*: spike density function calculated from the time series of *A* (window half-width: 0.2 s, Gaussian kernel). *C*: interspike interval (ISI) return map of the same neuron. *D*: Fourier spectrum calculated from a longer section of the spike density function (SDF) in *B*. The prominent peak at 1.8 Hz marks the frequency of the pyloric oscillation. *E*: quasiperiodic burst pattern of the PD neuron in response to sinusoidal forcing ($A = 1.0 \text{ nA}$). *F*: the SDF for the time series in *E*. This displays peaks with different amplitude due to local variations in the firing rate. *G*: the ISI return map of the forced PD neuron. Long intervals are scattered between 0.15 and 0.5 s. *H*: the Fourier spectrum of the SDF with multiple peaks. Asterisk marks the forcing frequency.

bursting during the whole duration of the recording. We excluded data from our analysis when the pyloric firing patterns were occasionally disrupted by cardiac sac events or other potent synaptic inputs arriving from other extraganglionic sources. The schedule of the experiments was as follows: we recorded the control activity of the neurons for 40–60 s, then applied the stimuli in separated 80- to 120-s trials allowing the cells to generate at least 100 bursts ($\approx 1,000$ spikes) per stimulation. The frequency and amplitude of the waveform was held constant during a trial.

Data analysis

Raw membrane potential data were visually inspected, while detailed quantitative analysis was performed using series of spike arrival times. Establishing the arrival times of action potential occurrences and constructing the spike train $\{t_i^s\} = \{t_0^s, t_1^s, t_2^s, \dots\}$ was achieved using the first time-derivative of the membrane potential $V_m(t)$ time series to determine its local maxima.

To characterize the spontaneous and stimulus-induced firing patterns, a number of functions and distributions were calculated from the spike time data. The spike density function (SDF) was used as a sensitive measure of the ongoing neuronal activity (Richmond et al. 1987; Szűcs 1998). The SDF provides a continuous estimate of the instantaneous firing rate and allows one to detect even slight modulations of the firing pattern (Paulin 1992). The SDF is calculated by convolving the time of each spike with a Gaussian-function $K(t)$, called a kernel

$$SDF(t) = \sum_i \int K(t' - t) \delta(t' - t_i^s) dt' = \sum_i K(t - t_i^s)$$

where $\delta(t)$ is the Dirac delta function, and $\int K(t') dt' = 1$. The half-width of the Gaussian was set to 0.2 s. Pyloric bursts of a regularly bursting PD neuron appeared as separated peaks in the SDF (Fig. 2*B*). The sampling resolution of the SDF was 0.02 s, providing at least 20 points per burst. Fourier analysis was used to detect and characterize any periodicities in the firing patterns. Fourier amplitude spectra were calculated from stationary parts of the SDFs before (control) and during sinusoidal forcing (trial). The amplitude of harmonics up to 5.0 Hz was calculated using 0.005-Hz resolution (rectangular window). To characterize the relative efficiency of the forcing current in modulating the firing patterns, we used the Fourier amplitude ratio. This parameter was computed as the ratio of the area under the principal peak of the forcing frequency to the area under the total spectrum (Richards et al. 1999).

Pyloric pacemaker neurons of the intact network exhibit short, periodic bursts of action potentials separated by silent periods of hyperpolarization. Hence bursts can be considered as the basic events of neural activity in the pyloric CPG. To characterize the timing of bursts, we located the onset of each burst and generated a subsequent discrete time series containing burst arrival times $\{t_i^B\} = \{t_0^B, t_1^B, t_2^B, \dots\}$. Here, the times of intraburst spike events were not taken into account. The burst onset time t_i^B was defined as the arrival time of the first spike in the successive bursts. We formulated a time series of burst cycle periods (BCP) by evaluating the time differences between burst initiations: $BCP(i) = t_{i+1}^B - t_i^B$. The dynamics of the bursting process is retained in the burst cycle period time series (Abarbanel 1996). As “proxy” coordinates for the state space of those dynamics, we may use the values of $BCP(i)$ themselves. The process is assumed to occur in a d -dimensional space with vector coordinates $\{BCP(i), BCP(i+k), BCP(i+2k), \dots, BCP[i+(d-1)k]\}$ at “time” i . The

time delay k is often taken to be unity, and while the dimension d may be larger than 2, for display purposes $d = 2$ is often selected. Data vectors such as this provide a state space in which many of the important dynamical properties of the underlying dynamics are retained. We created $d = 2$ state spaces (also called return maps) for the $BCP(i)$ time series by plotting points $[BCP(i), BCP(i + 1)]$ in a two-dimensional plane. Equilibrium or stable fixed points are seen as points in this plane along the 45° line. Period two orbits of the dynamics are seen as pairs of points in the plane, and more complex trajectories, higher order periodic orbits, or chaotic behavior produce more complex patterns. For comparison, we also constructed sequences and return maps of the interspike intervals: $[ISI(i), ISI(i + 1)]$, $ISI(i) = t_{i+1}^S - t_i^S$. The ISI return maps were used to demonstrate any changes in the dynamics of spike generation due to the periodic forcing. These graphs are effective tools for characterizing the timing of intraburst spikes.

Electronic model neuron

The electronic model neuron (EN) is an analog circuit implementation of a four-dimensional neuron model using ordinary differential equations with vector fields taken to be polynomials in the dynamical variables $[x(t), y(t), z(t), w(t)]$. The model takes the form

$$\begin{aligned} \frac{dx(t)}{dt} &= ay(t) + bx^2(t) - cx^3(t) - dz(t) + I \\ \frac{dy(t)}{dt} &= e - fx^2(t) - y(t) - gw(t) \\ \frac{dz(t)}{dt} &= \mu[-z(t) + S[x(t) + h]] \\ \frac{dw(t)}{dt} &= \nu[-kw(t) + r[y(t) + l]] \end{aligned} \quad (1)$$

where $a, b, c, d, I, e, f, g, \mu, S, h, \nu, k, r$, and l are adjustable parameters dependent on the underlying conductance based dynamics. $x(t)$ is the membrane potential of the model neuron, $y(t)$ is a fast current, $z(t)$, a slow current ($\mu \ll 1$), $w(t)$ represents the very slow ($\nu < \mu \ll 1$) intracellular exchange of calcium between its store and the cytoplasm (Falcke et al. 2000; Pinto et al. 2000), and I is the external current, sinusoidal in our case. The EN consists of four integrators, two multipliers, two adders, and two inverters and performs real-time computation of the differential equations (see Pinto et al. 2000 for details). We adjusted the internal parameters of the model (potentiometers) to obtain membrane potential oscillations closely resembling those of real biological neurons in intact pacemaker group, i.e., periodic bursting with 1- to 2-Hz frequency and 5–10 spikes per burst (see Fig. 11A). Unlike the intact pyloric neurons, the four-dimensional model produces spikes with larger amplitude than the depth of the interburst hyperpolarization. To obtain oscillations with realistic spike amplitude/hyperpolarization depth ratio, we reshaped the output of the circuit using an additional amplifier. We used two different gains, G_s and G_n , for the spikes and the hyperpolarized parts, respectively, G_n being larger than G_s .

RESULTS

Spontaneous firing patterns of neurons in the pyloric pacemaker group

Neurons of the intact pacemaker group (AB and 2 PDs) exhibited a regular oscillatory firing pattern (Fig. 2A) when the fast glutamatergic inhibition was blocked (with PTX in saline). The pacemaker neurons were therefore synaptically isolated from other pyloric neurons, but still continuously receiving

neuromodulatory inputs from anterior ganglia through the main stomatogastric nerve. The bursting frequency was 1.6 ± 0.3 Hz (mean \pm SD, $n = 25$). The two PD neurons and the AB neuron began and ended their bursts in synchrony, although individual spikes were not precisely synchronized (Elson et al. 1998). The monotonic bursting pattern was occasionally interrupted by intense activation of synaptic inputs associated with the cardiac sac rhythm. The frequency of these cardiac sac events tended to decrease during the recording sessions, thus allowing us to obtain long stationary sections of pyloric activity. Furthermore, as we show below, a low-frequency modulation of the pyloric oscillation was also routinely observed, as a consequence of interactions between the pyloric pacemaker neurons and the slower gastric (and/or esophageal) network.

The spike density function of the regularly bursting PD neuron is shown in Fig. 2B. The *SDF* consists of separate equidistant peaks of similar amplitude and shape reflecting the periodicity and precision of the repetitive firing pattern. The Fourier transform of a longer section of the *SDF* is shown in Fig. 2D (linear amplitude scale). A large peak at 1.75 Hz indicates the frequency of the intrinsic pyloric bursting rhythm f_{ib} ; the second harmonic at $2f_{ib} = 3.5$ Hz appears as a minor peak. This is a typical example of Fourier spectra obtained from pacemaker neurons in stable pyloric oscillation.

The interspike interval (*ISI*) return map of the PD neuron in the intact pacemaker group contains three separated clusters, which is a clear consequence of the repetitive bursting (Fig. 2C). Short *ISIs* associated with intraburst spikes are followed by a long *ISI* associated with the relatively longer interburst duration. A compact V-shaped cluster (at short intervals, ≈ 0.025 s) indicates precise and repetitive spiking in the successive bursts of the PD neuron.

Photoinactivation of the main pacemaker cell AB led to disruption of this regular activity and irregular spiking-bursting patterns in both the PD and other postsynaptic pyloric neurons ($n = 11$). Immediately after photoinactivation of AB, the PD expressed irregular spiking behavior that evolved into more regular bursting activity over a time scale of hours. The membrane potential of the irregularly bursting PD is shown in Fig. 3A, with the corresponding *SDF* in Fig. 3B. The Fourier transform of the *SDF* (Fig. 3D) is now predominantly broadband. As the firing pattern of these PD neurons tended to be more “bursty” over a longer time scale, the resulting Fourier spectra became more sharp and peaked. However, the precise periodic bursting seen in the intact pacemaker group was never restored.

In the low-frequency range of the spectrum, a single peak appears at 0.2 Hz, indicating some remaining periodicity in the spike train of the PD. This low-frequency rhythm was found in the majority of our preparations, and it is considered to be a synaptic modulatory effect from the gastric and/or esophageal network (Clemens et al. 1998; Russell and Hartline 1982).

ISI return maps of the PD neuron before (Fig. 2C) and after killing AB (Fig. 3C) show major differences. In the latter case no three-clustered structure is present, rather a scattered cloud of points appears. Here, we observe a mixture of short and long *ISIs* with no well-defined clusters.

The firing pattern of the isolated AB neuron is shown in Fig. 4A. Here both PD neurons were killed. The membrane potential trace of AB is similar to that of the PD in the intact pacemaker group but with smaller spikes. The AB retained its

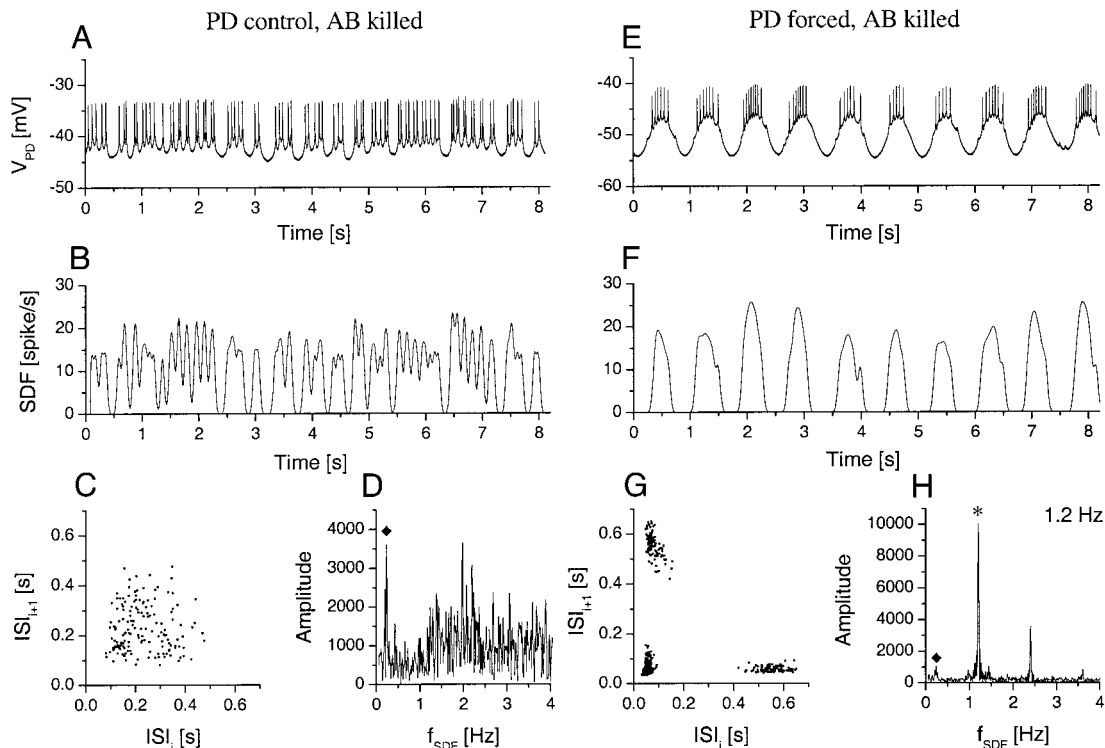


FIG. 3. PD neurons without AB exhibit irregular spiking/bursting patterns and can be regularized with sinusoidal forcing. *A*: irregular firing of a PD neuron shortly after the photoinactivation of AB. *B*: the corresponding *SDF* is aperiodic and random-like. *C*: diffuse *ISI* return map from the same neuron. *D*: broadband and “noisy” Fourier spectrum calculated from the *SDF*. The diamond symbol indicates a peak at 0.2 Hz, which appears to be the frequency of the intrinsic gastric rhythm. *E*: membrane potential of the forced PD neuron ($A = 1.0$ nA). *F*: the corresponding *SDF* reveals a nearly periodic pattern with a low-frequency envelope. *G*: triangular *ISI* return map of the spike train of *E*. *H*: Fourier transform of the *SDF*. The peak of the forcing frequency appears the largest (1.2 Hz). At 0.2 Hz the intrinsic low-frequency modulation is still clearly distinguishable and is marked by a diamond.

periodic bursting after photoinactivating the coupled PD neurons ($n = 4$), showing its fundamental role as a pacemaker in the pyloric rhythm. The frequency of the oscillation increased to ≈ 2.6 Hz from the normal $f_{ib} \approx 1.8$ Hz as shown by the Fourier-spectrum (Fig. 4D). A small peak indicating the modulatory influence of the gastric rhythm is present at 0.3 Hz as well as accompanying peaks on each side of the fundamental peak. These appear as the sum and difference of the pyloric and gastric frequency ($f_{ib} \pm f_{gastric}$). The *ISI* return map has three separate clusters (Fig. 4C) as that in the intact pacemaker group.

Effects of periodic forcing on various configurations of the pacemaker group

Sinusoidal currents $I_{sin}(t) = A \sin(2\pi ft)$ with A of order 0.5–2.5 nA had marked effects on the firing patterns and burst timing in all the neurons tested. The effect of the forcing current was most evident and clear on the neuron being injected. The other electrically coupled neurons followed the induced rhythm, but usually with smaller amplitude ratio at the forcing frequency.

Figure 2E shows the effect of $I_{sin}(t)$ with $A = 1$ nA and $f = 1.2$ Hz on the bursting activity of the PD neuron in intact pacemaker group. The interaction between the periodic forcing and the intrinsic pyloric oscillation resulted in a wide repertoire of burst patterns [$n = 174$ (8); number of trials (preparations)]. Comparing the Fourier spectra of spontaneously active (Fig.

2D) and forced (Fig. 2H) PD neurons, we find both similarities and differences. In this example, f was 1.2 Hz, less than f_{ib} . The original peak indicating the frequency of the intrinsic bursting frequency $f_{ib} \approx 1.9$ Hz is still evident, but additional peaks appear marking the frequency of the forcing current (1.2 Hz, asterisk) and its harmonics. Furthermore, linear combinations of the intrinsic and forcing frequencies appear as minor peaks (e.g., 0.7 Hz, or 3.1 Hz, $f_{ib} \pm f$) in the Fourier spectrum. These features are familiar characteristics of forced nonlinear oscillators. The *ISI* return map of the same neuron is shown in Fig. 2G. Long interspike intervals (e.g., those between successive bursts) now range from 0.15 to 0.5 s, resulting in long bands parallel with the axes. However, a compact cluster associated with the intraburst spikes is still visible near the origin of the map. The periodic forcing had only a minor effect on the intraburst spike pattern while strongly affecting the burst cycle periods.

The PD neuron was found to be far more flexible in response to the sinusoidal current injection when the AB was killed [$n = 110$ (3)]. Bursts of action potentials appeared during the depolarizing parts of the current stimulus; thus the firing pattern of the neuron became synchronized with $I_{sin}(t)$ (Fig. 3E), corresponding to 1:1 phase locking of activity. This entrainment occurred over a wide range of forcing frequencies (0.2–4.0 Hz). Fourier spectra calculated from the *SDF*s consist of a large peak at the position of the forcing frequency with a few higher harmonics (Fig. 3H). Interestingly, the minor peak at the position of the gastric frequency (0.2 Hz) is still observable,

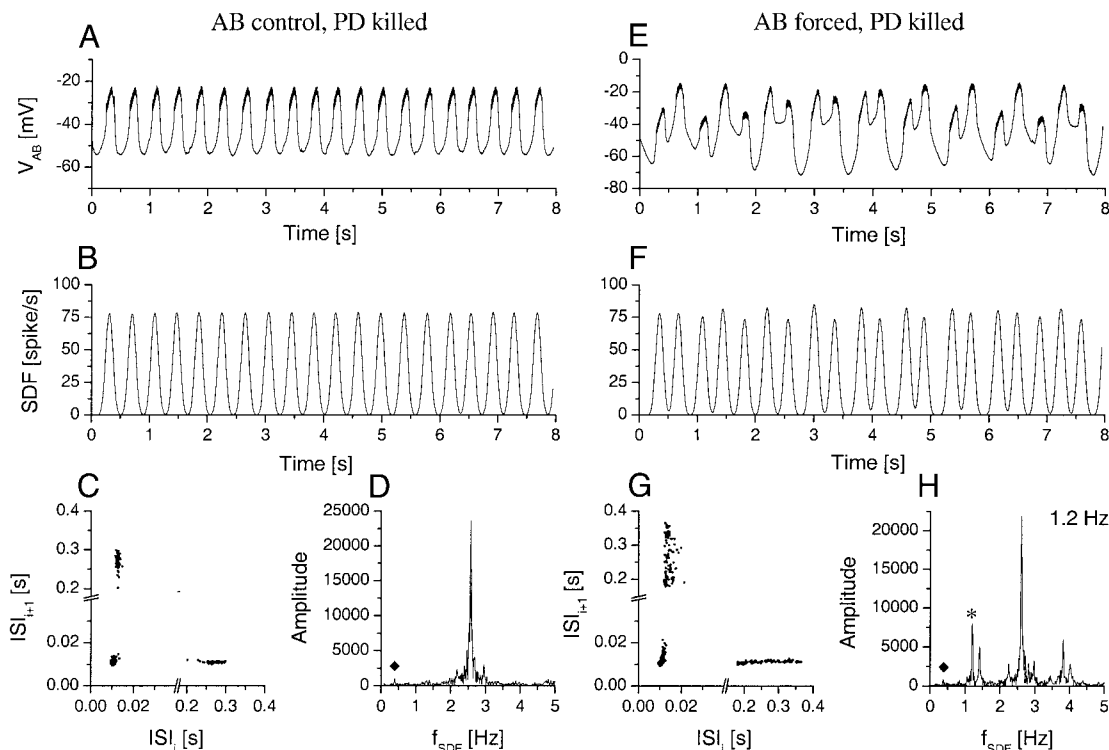


FIG. 4. The AB neuron maintains an oscillatory pattern in preparations with both PDs killed even in the presence of external periodic forcing. *A*: membrane potential of the isolated AB neuron. *B*: spike density function of *A*. *C*: *ISI* return map of the same neuron. *D*: Fourier spectrum calculated from a longer section of the *SDF* in *B*. The frequency of the pyloric oscillation was high, 2.6 Hz in this case. The low-frequency (gastric) peak is indicated by a diamond. *E*: complex burst pattern of the AB neuron during sinusoidal forcing at 1.4 Hz ($A = 2.0$ nA). *F*: the *SDF* for the time series in *E*. *G*: *ISI* return map. *H*: Fourier spectrum of the forced AB neuron. Linear combinations of the forcing frequency and the intrinsic rhythm appear as minor peaks.

demonstrating that neither killing the AB neuron nor the sinusoidal forcing eliminated or altered the gastric mill modulation. The return map constructed from the *ISIs* of this forced PD neuron is now three-clustered (Fig. 3*G*), similar to that seen with spontaneously bursting PDs in the intact pacemaker group. The cluster associated with the intraburst spikes, however, is more spread (0.04–0.15 s), showing that spike timing is less precise in this situation.

The firing pattern of the forced isolated AB neuron resembles that of the forced PD in the intact pacemaker group. Complex burst patterns emerged due to the interaction between the forcing and the intrinsic oscillation [Fig. 4*E*; $n = 99$ (2)]. The periodic forcing affected the timing of bursts more than that of the individual spikes within the bursts. The *ISI* return map is clearly three-clustered with a compact cluster at 0.01 s (Fig. 4*G*). Interburst intervals are spread between 0.2 and 0.4 s. The Fourier-amplitude spectrum of the forced AB neuron is quite rich with several peaks appearing at the position of the intrinsic pyloric rhythm, the forcing frequency, and their linear combinations (Fig. 4*H*).

Spike timing of forced pacemaker neurons: effect of varying stimulus frequency

We surveyed the firing patterns of the pacemaker neurons by changing the frequency and amplitude of the forcing current in small steps of 0.1 Hz and 0.5 nA, respectively. As part of the analysis, we calculated and compared *ISI* sequences from spontaneously active and from forced neurons. The effect of

$I_{\sin}(t)$ on the burst/spike timing of a PD neuron in the intact pacemaker group is shown in Fig. 5*A*. In control periods, $I(t) = 0$, the long interspike intervals show minor variations as a result of regular pyloric rhythm and stable burst cycle periods. On the contrary, complex *ISI* patterns arise when the neuron is responding to $I_{\sin}(t)$ (gray sections of Fig. 5*A*). The resulting *ISI* sequences have multimodal distributions. For larger f , 1:1 phase locking occurs when the neuron receives currents with $f \approx f_{ib}$, at 1.0 and 1.2 Hz here. As the precision of the burst timing increases, variations in the interburst intervals become smaller. The timing of intraburst spikes is far less affected by $I_{\sin}(t)$ than that of the bursts. At f higher than f_{ib} , a characteristic “skipping” behavior takes place. Many of the bursts of the PD are synchronized with the forcing current, being generated in the depolarized part of the sinusoidal waveform. Then, intermittently, a single burst is skipped, resulting in a lengthened interburst period (Fig. 5*A*, $f = 1.6$ Hz).

In contrast to the intact pacemaker group, when AB was killed, the PD neurons responded to periodic forcing with less precise and reproducible burst timing (Fig. 5*B*). In control periods, the *ISI* values are scattered, in contrast with the bimodal distribution characteristic of normal bursting neurons (Fig. 5*B*). Definition of bursts is troublesome in such neurons by using interspike data only. $I_{\sin}(t)$ injection altered the firing pattern of the PD neuron and induced nearly periodic bursting resembling normal pyloric activity. However, the burst timing of forced PD neurons was far less precise in preparations without AB than in the intact pacemaker group. This is clearly

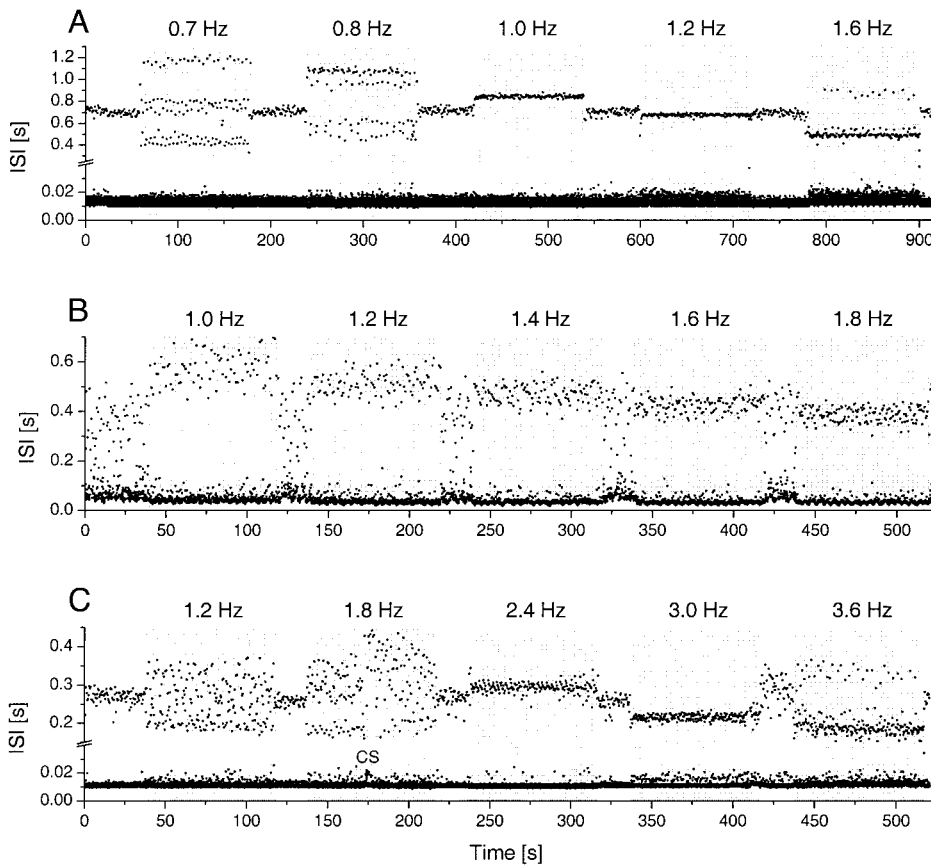


FIG. 5. The responses of the pacemaker neurons are strongly determined by the AB neuron and depend on the frequency of the forcing. *A*: *ISI* sequence of the spike train of a PD neuron in the intact pacemaker group. During the 900 s of experiment, 5 different forcing frequencies were used. These are indicated above the graph ($A = 1$ nA). A dense horizontal band of points indicates short *ISIs* during the episodes of high-frequency intraburst firing. Phase locking (1:1) appears at 1.0- and 1.2-Hz frequencies. *B*: *ISI* sequence of the PD spike train when AB was photoinactivated. There are large variations both in short and long interspike intervals indicating irregular bursting. Five different forcing frequencies between 1.0 and 1.8 Hz were used in separate temporal trials. *C*: similar to the above, but here the AB neuron was stimulated while the PDs were killed. The overall behavior of the AB neuron is similar to that of the PD in intact pacemaker group, but the variations in the values are somewhat larger. CS indicates a cardiac sac burst, which temporarily disrupted the bursting pattern of the neuron during the 1.8-Hz trial.

shown in Fig. 5*B*, where long interspike intervals are randomly distributed in a wide (0.2 s) region.

The *ISI* pattern of the isolated AB neuron was frequency dependent and multimodal, similar to that of the PD in intact pacemaker group, but more “noisy.” The *ISI* values of Fig. 5*C* are rather scattered; however, the different modes of synchronization and the skipping behavior (at 3.6 Hz) is still distinguishable.

Dynamics of burst timing and Fourier analysis of spike density data

Frequency-dependent effects on burst patterns were studied using *BCP* return maps as well as Fourier transforms of the spike density functions. A wide variety of responses occurred in pacemaker neurons forced at different frequencies. A typical example of the effects is shown in Fig. 6, where a PD neuron in the intact pacemaker group was stimulated using $I_{\text{sin}}(t)$ at seven different frequencies. The patterns in the $[BCP(i), BCP(i + 1)]$ plane display a gradual transformation as f is increased. At $f \ll f_{ib}$, loops and fixed points are observed (0.3, 0.4 Hz). The loops are indicators of quasiperiodic behavior. At $f = \frac{1}{2}f_{ib}$, 1:2 phase locking occurs, i.e., two bursts are generated during one period of the forcing waveform. Here a short burst cycle period is followed by a longer one, resulting in two compact densities on the return map, symmetrical to the 45° axis. Asymmetric return maps appear at moderate forcing frequencies (0.7, 0.8 Hz), slightly below that of the intrinsic bursting. Here a complex, possibly chaotic behavior emerges. However, the shapes appearing on the return map are still well defined and compact. As a result of the slight irregularities and

intrinsic noise present in the pyloric neurons, various phase-locking regimes can develop, and the burst pattern of the PD often jumps from one to another, e.g., from a 3:4 to a 4:5 mode and back. One-to-one phase locking is characterized by a very compact single fixed point on the diagonal of the graph when we set $f = 1.2$ Hz, close to that of the intrinsic oscillation. Skipping or intermittent behavior results in a three-clustered return map at higher stimulus frequencies (1.6 Hz), and then 2:1 phase-locking bursting can be observed (not shown). Development of irregular, possibly chaotic responses was also observed at yet higher stimulus frequencies ($f \geq 3$ Hz). A remarkable feature of all our *BCP* return maps is that each displays well-defined and compact forms (attractors), and has “forbidden areas” with no points inside.

Fourier spectra from the corresponding *SDF* data are displayed in Fig. 6*B*. At f below f_{ib} , the spectra are dominated by a number of distinct harmonics. In all cases we find a major peak close to the position of f_{ib} and another one at f . The positions of the smaller peaks appear as linear combinations of these two fundamental frequencies. Peaks evenly distributed along the frequency axis indicate precise $n:m$ phase locking, e.g., at 0.4, 0.5, or 1.2 Hz. “Noisy,” broadband Fourier-spectra (indicators of aperiodic or chaotic response) are obtained in the region below the 1:1 phase-locked mode (e.g., at 0.8 Hz here).

Without AB the response of PD to $I_{\text{sin}}(t)$ was far less rich and complex than that of the intact pacemaker group. $I_{\text{sin}}(t)$ induced periodic changes in the firing rate of the neurons rather than altering the timing of well-defined bursts (Fig. 7). At low f the arrival times of the irregular bursts show large, irregular

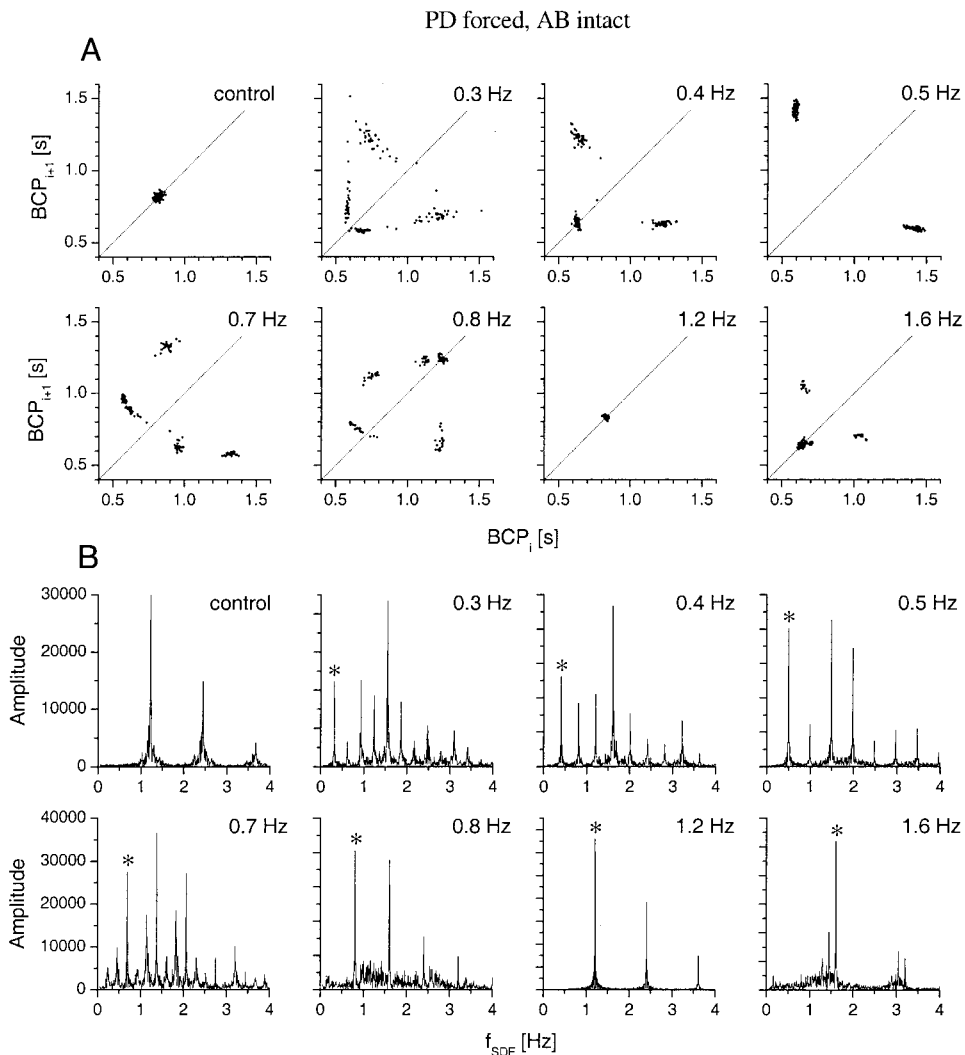


FIG. 6. PD neurons in intact pacemaker group show wide variety of responses to sinusoidal forcing. Burst cycle period (BCP) return maps (A) and Fourier spectra (B) of a PD neuron are shown in control and when forced at 7 different values of f . Each graph in A was constructed by plotting $[BCP(i), BCP(i + 1)]$. The forms show a strong dependence on f . Two fixed points appear at 0.5 Hz as a consequence of 1:2 phase locking. Phase locking (1:1) is obtained at 1.2 Hz resulting in a single fixed point on the 45° line in the $[BCP(i), BCP(i + 1)]$ plane. For f below $f \approx 1.0$ Hz, we see rather complex patterns in the $[BCP(i), BCP(i + 1)]$ plane. For larger f , we see more regular forced oscillations. B : the Fourier spectra calculated from various sections of the same spike train. Equidistant peaks in the diagrams at 0.4-, 0.5-, and 1.2-Hz frequencies indicate various $n:m$ phase-locked patterns. The asterisk indicates f . Another large peak near 1.6 Hz appears in several of the graphs indicating the frequency of the intrinsic pyloric rhythm.

variations resulting in dispersed point clouds on the BCP return maps (Fig. 7A, 0.5–0.7 Hz). A single fixed point appears for $f = 0.8$ Hz. The Fourier spectra calculated from the corresponding $SDFs$ show a similar tendency: a noisy baseline is present at lower frequencies (Fig. 7B, 0.5–0.7 Hz), then clear synchronization is indicated by a large peak (asterisk). One-to-one phase locking is clearly seen in each graph, and the dominant peak always appears at f . Minor peaks appear as higher harmonics. As noted above, a small peak appears at 0.2 Hz in each panel (diamond). This latter component is a result of the intrinsic gastric or esophageal modulation.

The autonomous firing pattern of the isolated PD neurons developed from nearly tonic spiking immediately after photo-inactivation of the AB to more bursty activity. Nevertheless, the observed synchronization effect was virtually independent of the spontaneous firing pattern of the isolated PD. The 1:1 phase locking was achieved equally when the PD neuron exhibited nearly tonic spiking or more regular bursting. The BCP graphs and Fourier analysis revealed flexible responses of isolated PDs in a wide range of frequencies and amplitudes of the applied current.

The response of the isolated AB neuron to changing f was in several aspects similar to that of the intact pacemaker group (Fig. 8). The BCP return maps show a gradual transformation

as the frequency of the injected current increases. One can identify quasiperiodic responses (0.5, 0.9 Hz), a near 1:2 phase-locked pattern, the complex dynamics at 2.0 Hz and 1:1 phase-locked behavior at 3.5 and 4.0 Hz. Here the intrinsic rhythm was unusually fast, close to 3 Hz (Fig. 8B, control). Fourier spectra show complex multiplets of peaks appearing at positions of the pyloric rhythm, the forcing frequency, and their linear combinations. The low-frequency gastric/esophageal modulation is also detectable (diamond).

Effects of changing the amplitude of the forcing current

To examine how the synchronization effect depended on the intensity of the periodic forcing, we changed the amplitude A of the injected current while holding the frequency f at constant values. We varied the amplitude of $I_{sin}(t)$ between 0.5 and 2.5 nA. The firing patterns exhibited a strong dependence on the amplitude of the forcing both in PD neurons in the intact pacemaker group and in isolated AB. Figure 9A shows the effect of different A and f on the amplitude ratio of a forced PD neuron (AB intact). At $A = 0.5$ nA, only a slight modulatory effect is observed. In this case the bursting of the pyloric cells remains quite regular; the position of the peak of intrinsic bursting is unchanged

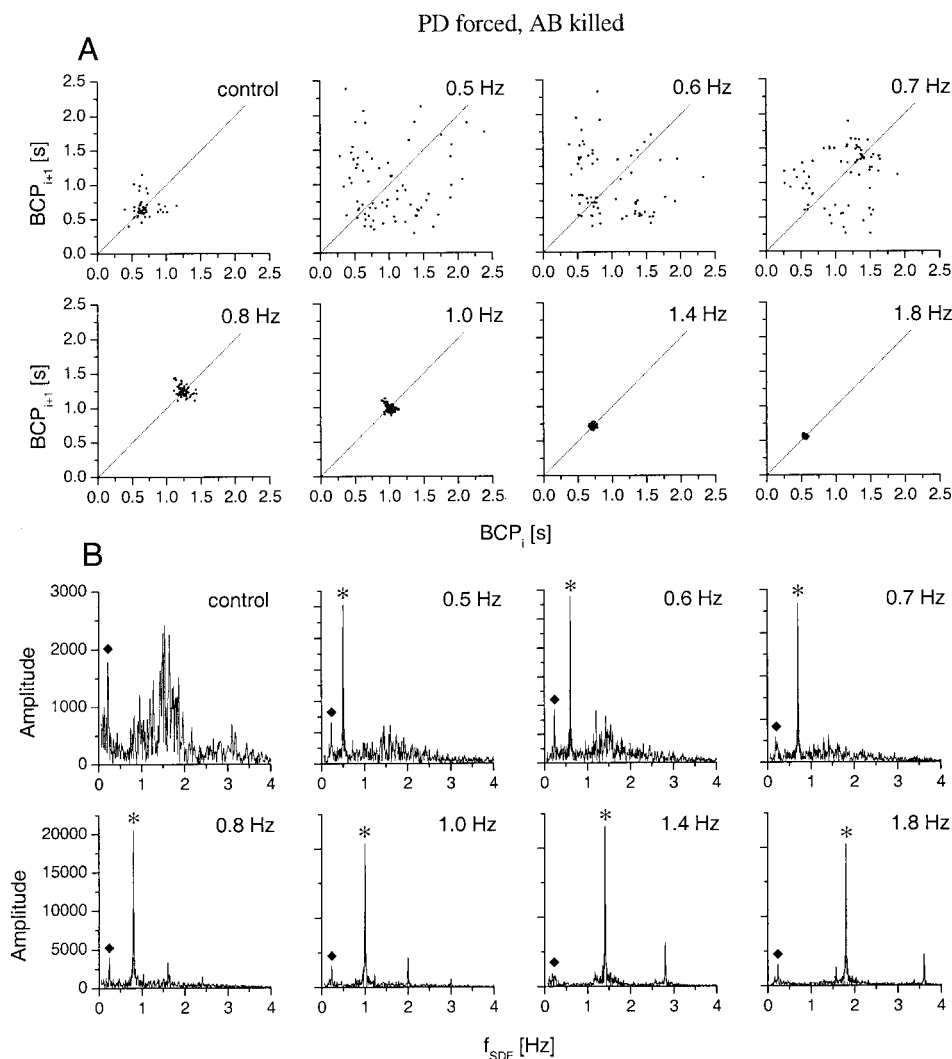


FIG. 7. The PDs respond to sinusoidal forcing in a flexible manner when the AB is killed. Burst cycle period maps and Fourier spectra are shown similar to that in Fig. 6, but AB was killed in this preparation. *A*: BCP return maps display a continuous transformation as the frequency of the forcing is increased: irregular scattered forms developing into a compact fixed point. Lack of additional point densities results from simple 1:1 phase locking and synchronized bursting. For f less than $f \approx 0.7$ Hz, we have generally complex and irregular behavior in the $[BCP(i), BCP(i + 1)]$ plane. For f above this, the 2 PD neurons can lock perfectly with the forcing. *B*: the corresponding Fourier spectra. All the graphs contain a large single peak at f , which is designated with an asterisk. The diamond marks the frequency 0.2 Hz of the intrinsic gastric modulation present in this preparation. This gastric modulation peak shows no dependence on f . The spectra are remarkably “smooth” above 0.7 Hz, when the forcing frequency becomes comparable with that of the original pyloric rhythm, observed before the elimination of AB.

and no phase-locking behavior is observed throughout the range of applied f . Consequently, the Fourier amplitude ratio of the forcing peak at all scanned frequencies is far less than that of the intrinsic oscillation. The Fourier ratio of the forcing is virtually independent of the applied frequency. A slight increase in the amplitude ratio is observed when setting the forcing frequency close to that of the pyloric bursting ($f = 1.6$ Hz, $f_{ib} = 1.7$ Hz here, arrow). In general, the Fourier spectra calculated from the $SDFs$ of PD neurons receiving low-amplitude current forcing resembled those obtained from spontaneously active pacemaker neurons receiving the intrinsic gastric/esophageal modulation (at 0.2–0.3 Hz). Next, as A is increased to 1.0 nA, the amplitude ratio of the forcing becomes larger, and 1:1 phase-locking appears at $f = 1.6$ Hz. Phase locking is indicated by the prominently high value seen in the panels (Fig. 9A, 1.0–2.0 nA). Simultaneously, the amplitude ratio of the intrinsic peak vanishes. What we observe here is the merging of the peak of the intrinsic rhythm with that of the forcing, and the two distinct peaks are replaced by a single large peak. Moreover, as the amplitude of the injected current is increased, the amplitude ratio of the forcing becomes larger at all applied frequencies, while that of the intrinsic peak becomes smaller.

The behavior of the isolated AB was similar to that of PD with intact AB (Fig. 9B). The amplitude ratio of the stimulus frequency increased with the intensity of the forcing, while that of the intrinsic frequency changed in an opposite manner. Phase-locking (1:1) occurred at $f = 2.4$ Hz with $A = 0.5$ nA first, then at 3.0 Hz, when $A = 1.5$ nA. The amplitude ratio of the forcing was a monotonously increasing function of the current amplitude at all frequencies.

This kind of analysis was performed using the data from PDs of the intact pacemaker group and isolated AB neurons. Since the isolated PD neurons showed no autonomous bursting after killing the AB, no pyloric peak appeared in the Fourier spectra. Phase-locking behavior (1:1) developed in a wide range of frequencies (0.2–3.0 Hz). This phenomenon was virtually independent of the amplitude of the injected current. The isolated PD neurons developed an irregular bursting behavior some time after killing the AB (>1 h). The Fourier spectra of the $SDFs$ of such neurons contained a wide and “noisy” peak and broadband baseline. Nevertheless, the injection of sinusoidal current removed the wide intrinsic peak and resulted in spectra similar to those in Fig. 7.

Various modes of activity of the PD/AB neurons are displayed on the frequency-current amplitude map of Fig. 10. Here, the frequency of the sinusoidal current was nor-

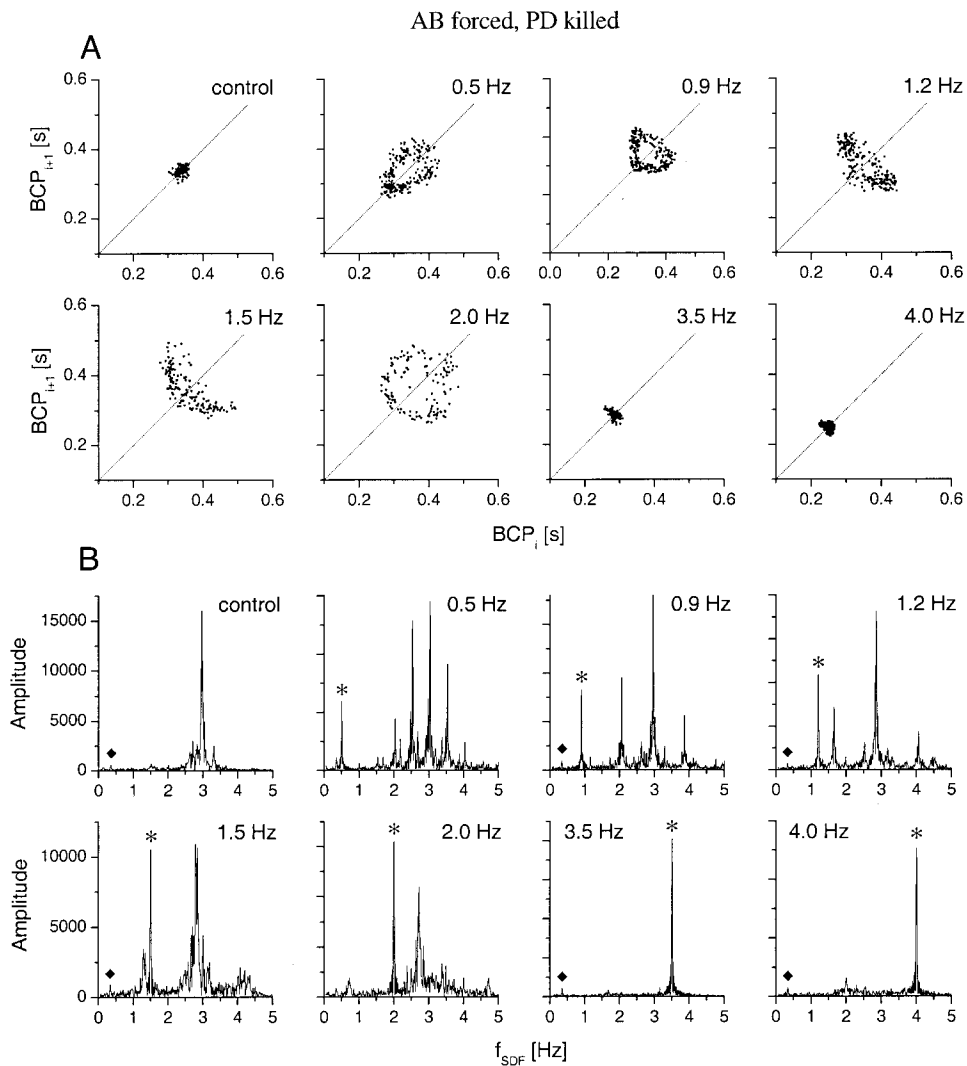


FIG. 8. The isolated AB neuron exhibits robust responses to sinusoidal forcing. *BCP* return maps (A) and Fourier spectra (B) of AB are displayed when both PDs were eliminated. A: gradual transformation of the forms of the return maps can be seen as f is increased. Two dense clusters appear at 1.2 Hz, close to the position of 1:2 phase-locking. Phase locking (1:1) is obtained at 3.5- and 4.0-Hz frequencies, due to the fast autonomous oscillations in this AB (≈ 3 Hz). B: the Fourier spectra calculated from the *SDF* data. At 0.5 Hz we obtain 1:6 phase-locked patterns indicated by the equidistant peaks and the ratio between the forcing frequency and the intrinsic one. Noninteger relationship between the fundamental peaks suggests quasiperiodic or irregular behavior as seen at 0.9–2.0 Hz. Above, 1:1 phase-locking appears. The intrinsic gastric modulation is observable in all spectra.

malized to the frequency of the intrinsic (pyloric) bursting. Each symbol represents a single experimental trial and corresponds to the different modes of operation. This presentation of the responses is called a phase-diagram or Arnol'd-map (Glass et al. 1986; Hayashi and Ishizuka 1995). The zones of 1:1 and 1:2 phase locking have a conelike shape, the Arnol'd tongue. Each phase-locking zone possesses its own Arnol'd tongue, but here, for practical reasons, only two are displayed. Complex dynamics and aperiodic patterns occur between the tongues.

The Arnol'd map of the isolated AB neuron is shown in Fig. 10B. The overall response of the isolated AB neuron is similar to that of the whole pacemaker group, but the zones of synchronization are slightly wider here. Although the indicated frequencies are normalized values, i.e., frequency of the intrinsic bursting of each neuron was taken into account, the current values are not normalized. Since the same amount of current can evoke slightly different responses in neurons of the same type (e.g., PD) but from different animals, it is difficult to define the exact shape of the tongues in the averaged graph. However, these maps show similarities to those obtained from “noiseless” theoretical models (Aihara et al. 1984; Stiber et al. 1997).

Responses of the electronic model neuron to periodic forcing

The electronic model neuron was subjected to the same type of periodic forcing, as the biological neurons. The autonomous periodic bursting pattern of the four-dimensional EN is shown in Fig. 11A. The frequency of the pyloric-like oscillation was set close to 2 Hz (Fig. 11D). Due to the precisely periodic character of the pattern, the *ISI* return map consists of only six points, equal to the number of spikes emitted per burst (Fig. 11C). Actually, the six “points” are clusters of overlapping points. When driving the EN with $I_{sin}(t)$ with $A = 2$ nA, $f = 1.4$ Hz, the burst pattern became slightly irregular and both the timing of the bursts and the number of emitted spikes were influenced. This is clearly seen as variations of the *SDF* in Fig. 11F. The *ISI* return map of the forced EN is similar to that of the forced PDs or AB, i.e., the variations in the long interburst values increased, but the short *ISI* cluster remained more or less unaltered (Fig. 11G). The Fourier amplitude spectrum of the forced EN has a broadband baseline and several peaks as a consequence of the interplay between the intrinsic rhythm and the forcing (Fig. 11H).

The frequency dependence of the forcing effect is shown in the Fig. 12. *BCP* return maps (Fig. 12A) reveal subharmonic

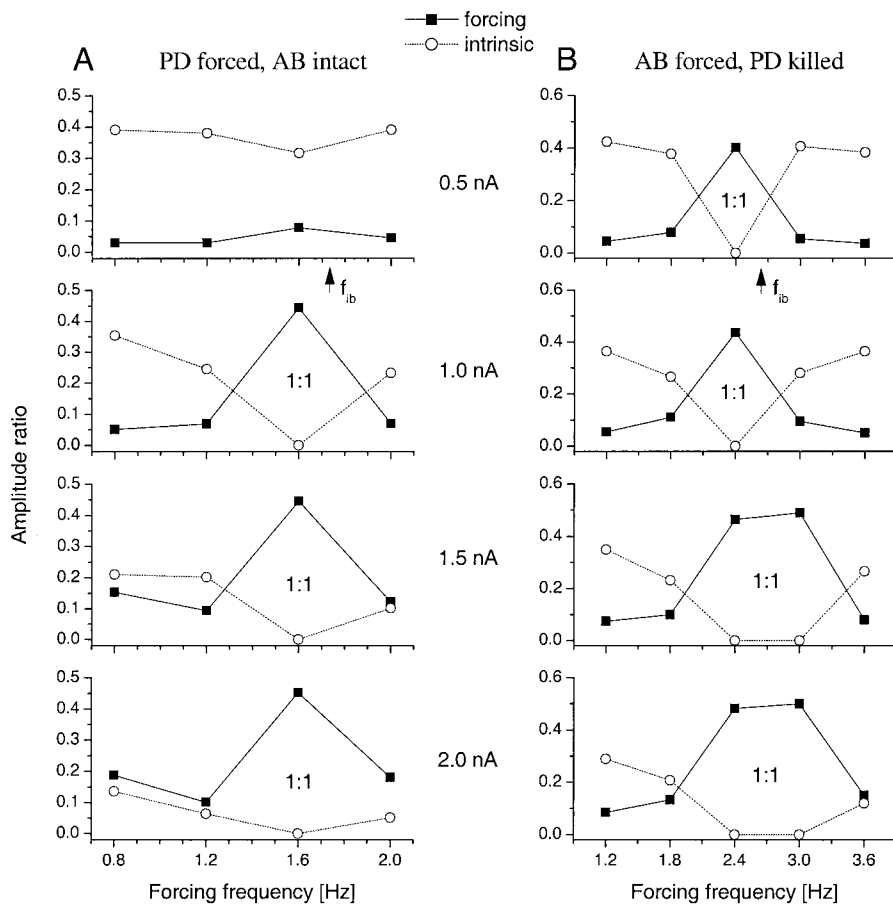


FIG. 9. The amplitude ratio (a.r.) of the forcing shows a plain monotonous dependence on the magnitude of the injected current and has a reverse relationship with the a.r. of the intrinsic oscillation. A: here, the PD neuron was sinusoidally forced with AB intact in the preparation. The magnitude of the sinusoidal current is indicated between the panels. Squares, a.r. of the forcing; open circles, a.r. of the intrinsic oscillation. Increasing the current amplitude leads to 1:1 phase locking, resulting in a single peak at the position of the forcing frequency (at 1.0 nA and above). B: same as A, but here the AB was forced and both PDs eliminated. The zone of the 1:1 phase locking is wider here. Arrows indicate the frequency of the intrinsic pyloric oscillation (f_{ib}). Clearly, the 1:1 phase-locking zone appears near the position of f_{ib} .

and superharmonic synchronization (0.5, 1.0, and 2.0 Hz) or chaos (0.4 and 1.4 Hz), depending on the ratio between the f and the intrinsic frequency. Accordingly, Fourier spectra contain either equidistant peaks or linear combinations of the two fundamental frequencies with broadband baseline. The response at 2.6 Hz resembles the skipping behavior of the forced PD neuron in the intact pacemaker group to the extent that there are three densities of points; however, these are arcs rather than well-defined and separated clusters. Clear quasi-periodic or skipping (escape) responses were not observed in the EN; instead, high-order $n:m$ synchronization with very long periods or chaotic responses were found. We explain this observation as a consequence of the low amount of intrinsic noise and high stationarity of the EN. Switching between different $n:m$ modes and skipping behavior were frequently seen in lobster pacemaker neurons, while the dynamics of the EN often evolved along a chaotic attractor.

DISCUSSION

There is increasing evidence that neural networks at different levels of complexity can operate in a coherent fashion as a result of synchronization (Destexhe et al. 1996; Golomb et al. 1994; Gray et al. 1989; MacLeod et al. 1998). Even in individually irregular neurons, synchrony and entrainment have been observed (Elson et al. 1998, 1999; Rabinovich et al. 1997). Experimental studies as well as computational models show that single neurons can exhibit a wide variety

of behavior including synchronization of bursts/spikes, harmonic or subharmonic synchronization, quasiperiodicity, and chaotic oscillations (Aihara et al. 1984; Hayashi et al. 1982). Entrainment and chaotic responses have also been demonstrated in very complex systems such as large populations of neurons with complex interconnections (Hayashi and Ishizuka 1995).

In this paper we have experimentally investigated synchronization phenomena in a small network of electrically coupled neurons. Detailed understanding of synchrony and regularity in oscillations of this kind of network is important and required to interpret mechanisms of information processing in such networks as well as in larger ones. Since CPGs play a substantial role in homeostatic regulation of an organism, it is important to explore and interpret the responses of such networks to external perturbations or endogenous rhythmic drives.

The pyloric pacemaker group of the stomatogastric nervous system offers an especially propitious opportunity for studying synchronization phenomena, since the architecture and function of this circuit is well described. This means that detailed modeling of the circuit is possible both in numerical simulations and in analog electrical circuitry (Pinto et al. 2000; Szűcs et al. 2000). Furthermore, as these networks and their ability to produce rhythmic output from a collection of component neurons with complex dynamics becomes understood, similar approaches can be carried out in realistic interpretations of larger networks in vertebrates.

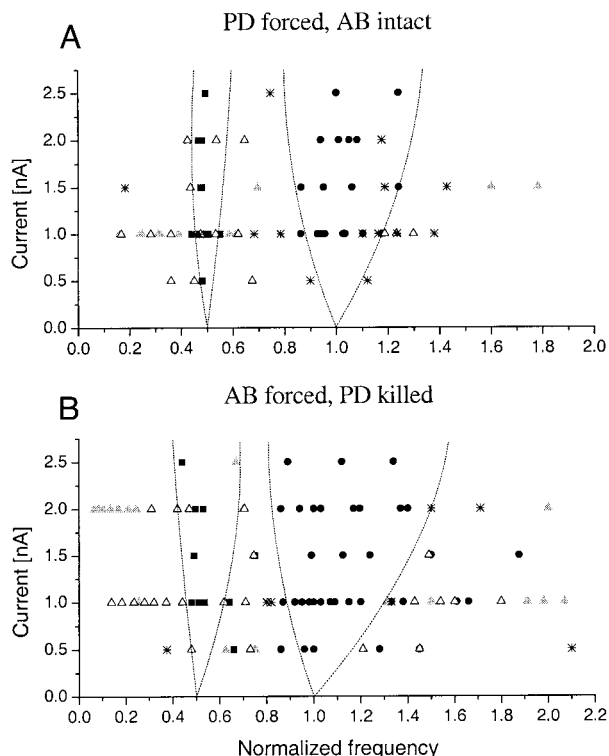


FIG. 10. The Arnold's maps of the forced intact pacemaker group and the isolated AB show zones of synchronization and complex behavior. *A*: stability/instability in the (A, f) plane for the bursting modes of the pacemaker neurons when forced by $I_{\sin}(t)$. The f is normalized to the intrinsic bursting frequency. Symbols represent various bursting/firing modes: filled circles, 1:1 phase locking; filled squares, 1:2 phase locking; filled triangles, other $n:m$ phase-locked patterns; open triangles, quasiperiodic responses; stars, irregular/chaotic patterns. Two zones of synchronization are depicted in each panel: the 1:1 phase-locking and 1:2 phase-locking zones. *B*: responses of the isolated AB neuron. When both PDs were killed, the responses of the AB neuron alone led to wider zones of synchronizations than with all pacemaker neurons intact.

Intrinsic oscillations and periodic inputs in neuronal networks

There have been earlier studies on the stomatogastric nervous system involving periodic stimulation of nerve cells. Ayers and Selverston (1979) used existing synaptic inputs of both excitatory and inhibitory type to stimulate the pacemaker neurons in a periodic manner (the pacemaker group was not pharmacologically isolated). The synaptic stimulation elicited large variations in the arrival times of the pyloric bursts, and a relatively narrow 1:1 synchronization zone was found. Other studies involved intracellular current injection of rectangular waveforms. Hooper (1998) revealed a clear graded relationship between the burst delay of pyloric PY neurons (in 1:1 synchronized mode) and the temporal parameters of the waveform defining the rectangular waveform. These results suggest that the PY neurons can transduce temporal patterns into neural code. Elson and coauthors (Elson et al. 1999) used synaptically isolated lateral pyloric neurons and examined the dependence of the regularization effect on the polarity and temporal characteristics of the injected rectangular waveform. To our knowledge, various types of entrainment of neuronal bursting activity by sinusoidal current injection have not previously been demonstrated either in the crustacean pyloric pacemaker network or in any other similar small group of electrically coupled neurons.

In a few experiments we compared the effect of sinusoidal current waveforms to that of rectangular pulse trains used in earlier studies. We took the frequency and amplitude of the rectangular pulses to be equivalent to those of the sinusoids. We found that the extent and precision of the effect on burst timing and spike density was significantly greater with sinusoidal waveforms than with rectangular pulse trains. Fourier spectra of pyloric neurons under stimulation with rectangular waveforms were more broadband and the harmonics less well defined. It is known that synaptic neurotransmission between stomatogastric neurons is of a graded type (Graubard et al. 1980), thus the synaptic currents received by the nerve cells contain slowly varying components (Manor et al. 1997). The main feature of the sinusoidal current waveform may well be its lack of the high-frequency components found in the rectangular pulses.

In about half of our preparations we detected a characteristic low-frequency component in the firing patterns of pyloric pacemaker neurons. This modulation possibly originates from an inhibitory coupling from the gastric MG neuron to the AB/PD assembly (Clemens et al. 1998). Since PTX as a blocker of fast inhibitory connections was used in all of our experiments, and the gastric modulation was present, this inhibitory synapse is probably not of the fast glutamatergic type (Cleland and Selverston 1998).

Our results also raise an issue regarding the interaction between distinct periodic oscillatory pattern generators. As seen in many experiments, the low-frequency and low-amplitude sinusoidal current did not worsen the precision of the intrinsic pyloric oscillation; rather, a subharmonic (e.g., 1:5) synchronization took place. Analogously, the low-frequency gastric modulation can act as a regularizing factor on the pyloric rhythm. The reverse effect, i.e., the regularization of the gastric rhythm by the fast pyloric oscillation has already been elegantly demonstrated in crabs (Bartos et al. 1999).

Variations in the timing of pyloric bursts as well as in the alterations in the number of emitted spikes are possible ways of information processing in the pyloric CPG. The various temporal patterns of burst activity revealed by return maps show stable frequency-dependent output responses to periodic forcing. These temporal forms displayed notable long-term stability and consistency during the periodic forcing, especially in the intact pacemaker group. In this respect, the temporal forms and various entrainment zones were similar to those found in periodically driven PY neurons described by Hooper (1998). The pyloric pacemaker neurons transduce incoming temporal patterns (here, sinusoidal waveforms) into stationary neural codes, thus representing a form of information storage (Golowash et al. 1999; Matsugu et al. 1998).

In our experiments, intermittent or chaotic responses were observed only in a narrow range of stimulus parameters showing that the intact pyloric pacemaker can maintain a long-term stable oscillation and has a tendency to express periodic patterns even in the presence of such external perturbations. Termination of the current injection quickly led to restoration of the original pyloric rhythm in the intact circuit, i.e., the burst patterns were virtually indistinguishable before and after the forcing. Even extended (up to 15 min) periodic forcing did not induce any aftereffects in the firing patterns, phase shifts, or reconfiguration of the intact pyloric network. It is indeed one of the important observations of the current work that the rhyth-

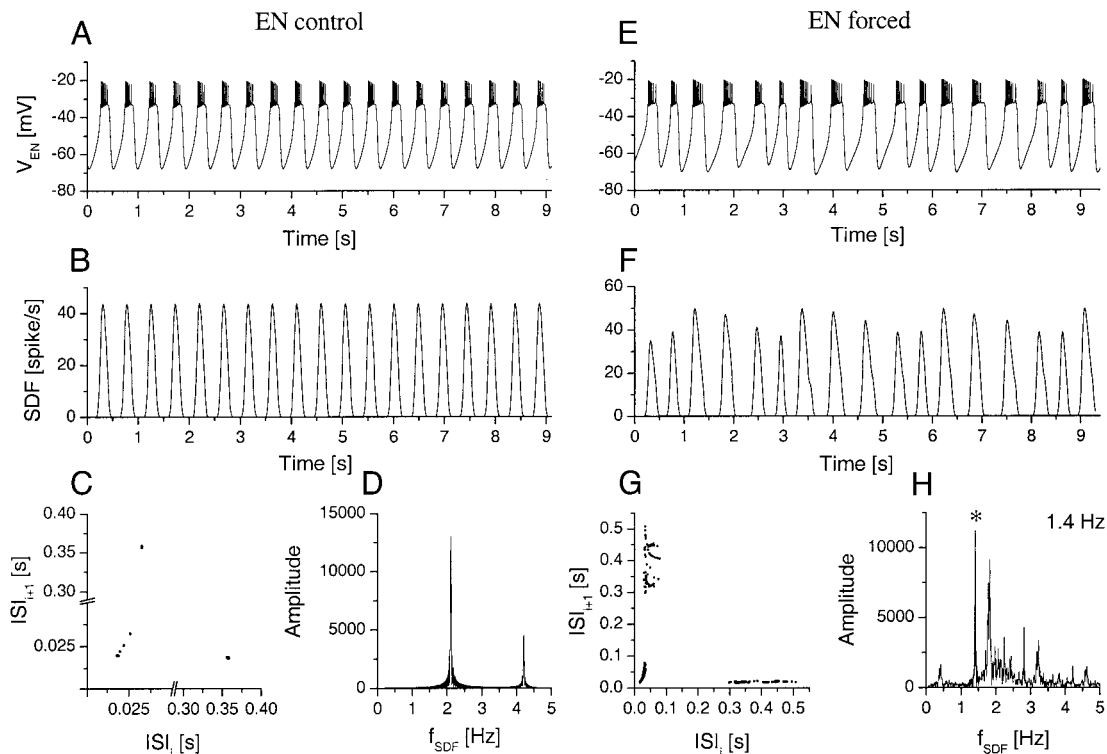


FIG. 11. The electronic model neuron (EN) mimics several aspects of the voltage activity of real pyloric neurons. *A*: the output of the 4-dimensional model neuron, with the $x(t)$ variable reshaped by a nonlinear amplifier. The pattern is similar to that seen in real bursting pacemaker neurons. *B*: *SDF* of *A*. *C*: *ISI* return map of the periodically bursting EN ($f_{ib} = 2.1$ Hz). *D*: the Fourier spectrum calculated from the *SDF*. *E*: the firing pattern of the sinusoidally forced EN ($f = 1.4$ Hz). The bursts are not uniform and burst cycle periods show variations. *F*: corresponding *SDF*. *G*: *ISI* return map of the forced EN. Long *ISIs* (i.e., interburst intervals) range from 0.3 to 0.6 s. The Fourier spectrum of *H* has both narrow peaks and a broadband component—indication of a complex or chaotic response.

micity and stationarity of the pyloric oscillation is well preserved under the influence of long-term external periodic perturbations. In these circumstances the pyloric network shows no signs of plasticity induced by the forcing.

Intact pacemaker group versus reduced configurations

The spontaneous behavior of the pyloric pacemaker group as well as its response to periodic forcing were completely different when the main pacemaker neuron AB was present and when it was removed by photoinactivation. It appears then that rich dynamical behavior, phase-locking, numerous zones of synchronization, and quasiperiodicity are characteristics of the intact pyloric pacemaker group only. When AB is killed, the PD neurons remain able to spike and burst, but in a more irregular manner than in the intact pacemaker group (Bal et al. 1988; Elson et al. 1998). Their activity can evolve from tonic firing, through irregular spike generation, to clear (but still irregular) bursting. The basis for this change in activity is unclear. It may reflect recovery from nonspecific damage (with increased leakage currents) following the death of the coupled AB cell; alternatively, it could also result from an intrinsic, activity-dependent modulation of membrane conductances (Turrigiano et al. 1995). The time course of the transformation of firing patterns in isolated PD neurons (hours) is faster than that in cultured stomatogastric neurons (days). Regardless of their activity pattern, however, the remaining PD neurons show simplified, flexible responses (phase locking) to external stim-

uli. On the other hand, when the PDs are killed, AB retains strong oscillatory properties (although with less stability and stationarity than the intact pacemaker). Compared with the isolated PDs, AB shows a narrower range of phase locking. The combination of rich dynamical function and flexibility therefore depends on the cooperative behavior of the three neurons. AB is the robust part of the pacemaker, while the two PD neurons are clearly the flexible ones.

Taken together, the intact pyloric pacemaker group of neurons is functioning as an optimized, single, low-dimensional oscillator capable of both initiating a stable motor pattern and responding to time-varying signals. The intact group exceeds in performance all other reduced configurations of the pacemaker neurons.

Motivations and benefits of the spike density function technique

In our study we analyzed in detail spike time data, while raw membrane potential time series were only visually inspected. This approach is supported by several arguments. First, spikes, rather than slow-wave membrane oscillations control the output of pyloric muscles. The evolution of the membrane potential of single neurons is of small significance in controlling muscle activity. The motor response depends on the number and temporal patterns of spikes of the presynaptic neurons (Morris and Hooper 1997). Second, there is a roughly monotonous relationship between the instantaneous firing rate of the

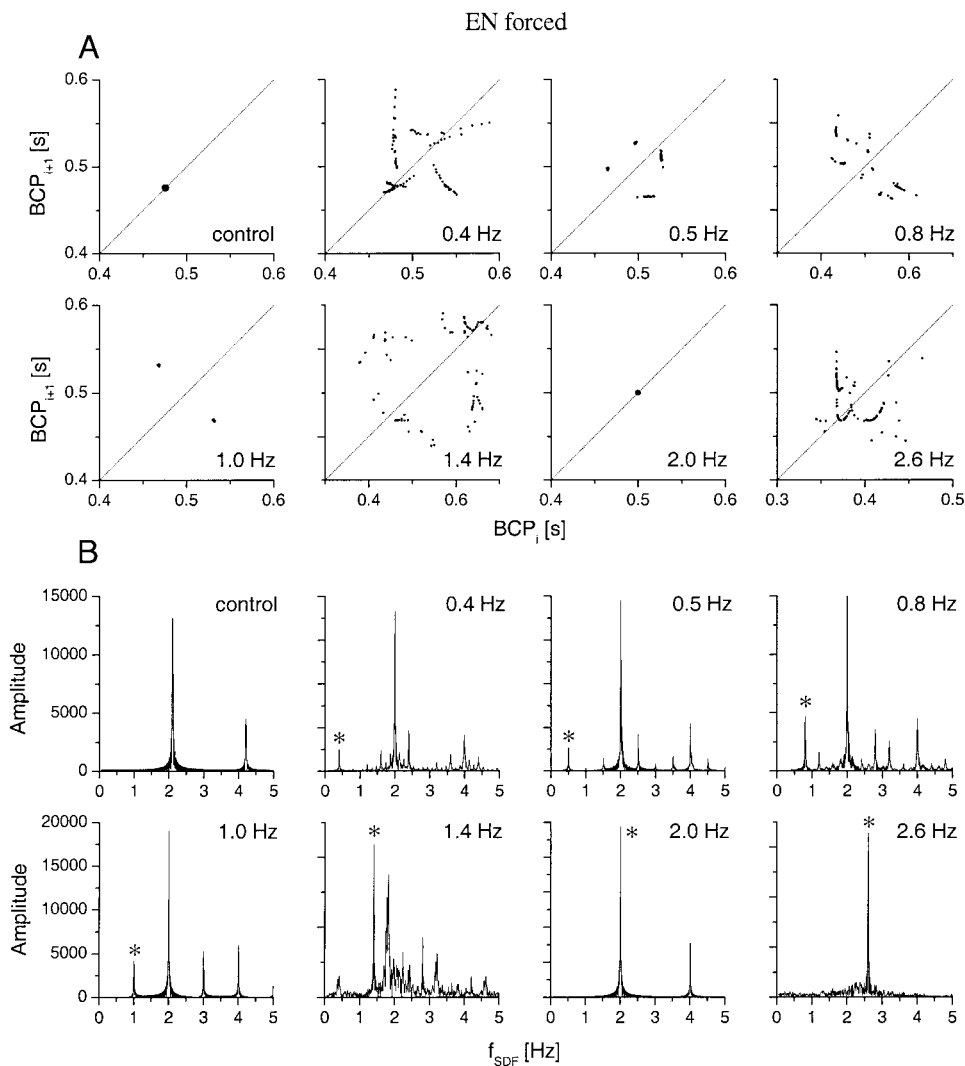


FIG. 12. The EN exhibits rich nonlinear behavior similar to that seen in forced pacemaker neurons and shows strong dependence on the frequency of the forcing. *A*: *BCP* return maps in control and using 7 different frequencies (f indicated on each panel, $A = 2$ nA). The forms appearing on the panels are either very compact fixed points or diffuse attractors. In control the behavior is periodic with a single fixed point on the diagonal. Slightly noisy 1:4 phase-locking response is observed at 0.5 Hz, while clear 1:2 phase locking is achieved at 1.0 Hz. Chaotic responses appear at 0.4, 1.4, and 2.6 Hz, while 1:1 synchronization is seen at 2.0 Hz. *B*: Fourier amplitude spectra of the corresponding *SDFs*. Broadband spectrum appears at 1.4 Hz, indicating irregular behavior, while at other frequencies the intrinsic peak locks to 2.0 Hz, indicating a tendency for various types of $n:m$ phase locking.

neuron and the actual membrane potential meaning that the active depolarized periods of bursts can be clearly identified by knowing the arrival times of spikes or equivalently, the instantaneous firing rate. Spike density therefore suitably represents the bursting activity of pyloric cells or other types of neurons displaying plateau potentials.

The computed *SDF* function reveals fine modulations in the firing pattern, which are not easily recognizable in the original time series (e.g., gastro-pyloric interaction). Fourier analysis of the *SDFs* provides a further efficient way to characterize the spike trains and interactions between rhythmic networks. The amplitude and width of the peaks as well as the overall shape of the spectrum clearly shows the most important temporal features of the firing patterns.

Variations in the input resistance and size of the pacemaker neurons as well as the relative position of the current injecting electrode made it somehow difficult to average and statistically analyze data obtained from different animals. Zones of synchronization and irregular dynamical behavior were evident and well defined when altering the frequency and amplitude of $I_{sin}(t)$ using the same preparation and configuration. However, the magnitude of the effects varied among different preparations. Normalization of the current frequency was straightforward across preparations as the frequency of the intrinsic

pyloric oscillation offered a reference value for each measurement. Similar simple normalization technique for the current amplitude (or current density) could not be performed.

Low dimensional oscillatory dynamics in models and biological neurons

Despite the enormous biophysical and biochemical complexity of living neurons, they can express low-dimensional behavior. In this case the evolution of the membrane potential, the most commonly measured state variable of the neuron, depends on the interaction of a small number (3–5) dynamical variables (Falcke et al. 2000; Rabinovich et al. 1997). Equivalently, the time evolution of the membrane potential and the other variables can be described using the same number of differential equations; however, the exact form of the equations might be unknown. The behavior and interactions of individual neurons are still determined by a large number of cooperating biophysical and metabolic processes. These processes, however, can be combined into a small number of abstract dynamical variables, like those appearing in the Hindmarsh-Rose model. Bursting activity of motor pattern generating neurons can well be described using the simplistic polynomial models. Although the cooperative behavior of the network is a periodic

oscillation, some of the individual neurons, when isolated from their counterparts, can display chaotic firing patterns (Elson et al. 1998; Rabinovich et al. 1997).

Our earlier results have shown that a simple four-dimensional model reproduced significant functional aspects of individual pyloric neurons with regard to membrane voltage activity. Depending on the setting of internal coefficients and current offsets, the EN can generate periodic or chaotic bursting or tonic spiking. In further experiments this EN displayed a remarkable ability to interact cooperatively with living pyloric CPG neurons: the electronic model neuron was connected to synaptically isolated PD neurons via dynamic clamp, and together they produced regular oscillatory patterns similar to those in intact pyloric networks (Szűcs et al. 2000). The experiments reported here give further support to the use of low-dimensional polynomial models to simulate networks of biological neurons.

We thank R. Pinto and G. Stiesberg for constructing and calibrating the electronic neuron model.

Partial support for this work came from the U.S. Department of Energy, Office of Basic Energy Sciences, Division of Engineering and Geosciences, under Grants DE-FG03-90ER14138 and DE-FG03-96ER14592, and from the Office of Naval Research under Grant ONR N00014-00-1-0181.

REFERENCES

- ABARBANEL HDI. *Analysis of Observed Chaotic Data*. New York: Springer, 1996.
- AIHARA K, MATSUMOTO G, AND IKEYAGA Y. Periodic and non-periodic responses of a periodically forced Hodgkin-Huxley oscillator. *J Theor Biol* 109: 249–269, 1984.
- AYERS JL AND SELVERSTON AI. Monosynaptic entrainment of an endogenous pacemaker network: a cellular mechanism for von Holst's magnet effect. *J Comp Physiol* 129: 5–17, 1979.
- BAL T, NAGY F, AND MOULINS M. The pyloric central pattern generator in crustacea: a set of conditional neuronal oscillators. *J Comp Physiol* 163: 715–727, 1988.
- BARTOS M, MANOR Y, NADIM F, MARDER E, AND NUSBAUM MP. Coordination of fast and slow rhythmic neuronal circuits. *J Neurosci* 19: 6650–6660, 1999.
- BARTOS M AND NUSBAUM MP. Intercircuit control of motor pattern modulation by presynaptic inhibition. *J Neurosci* 17: 2247–2256, 1997.
- BIDAUT M. Pharmacological dissection of pyloric network of the lobster stomatogastric ganglion using picrotoxin. *J Neurophysiol* 44: 1089–1101, 1980.
- CALABRESE RL. Cellular, synaptic, network, and modulatory mechanisms involved in rhythm generation. *Curr Opin Neurobiol* 8: 710–717, 1998.
- CANAVER CC, CLARK JW, AND BYRNE JH. Simulation of the bursting activity of neuron R15 in *Aplysia*: role of ionic currents, calcium balance, and modulatory transmitters. *J Neurophysiol* 66: 2107–2124, 1991.
- CHILLEMI S, BARBI M, AND DI GARBO A. Dynamics of neuronal discharge in snail neurons. *BioSystems* 40: 21–28, 1997.
- CLELAND TA AND SELVERSTON AI. Inhibitory glutamate receptor channels in cultured lobster stomatogastric neurons. *J Neurophysiol* 79: 3189–3196, 1998.
- CLEMENS S, COMBES D, MEYRAND P, AND SIMMERS J. Long-term expression of two interacting motor pattern-generating networks in the stomatogastric system of freely behaving lobster. *J Neurophysiol* 79: 1396–1408, 1998.
- DESTEXHE A, BAL T, McCORMICK DA, AND SEJNOWSKI TJ. Ionic mechanisms underlying synchronized oscillations and propagating waves in a model of ferret thalamic slices. *J Neurophysiol* 76: 2049–2070, 1996.
- ELSON RC, HUERTA R, ABARBANEL HDI, RABINOVICH MI, AND SELVERSTON AI. Dynamic control of irregular bursting in an identified neuron of an oscillatory circuit. *J Neurophysiol* 82: 115–122, 1999.
- ELSON RC, SELVERSTON AI, HUERTA R, RULKOV NF, RABINOVICH MI, AND ABARBANEL HDI. Synchronous behavior of two coupled biological neurons. *Physiol Rev Lett* 81: 5692–5695, 1998.
- FALCKE M, HUERTA R, RABINOVICH MI, ABARBANEL HDI, ELSON RC, AND SELVERSTON AI. Modeling observed chaotic oscillations in bursting neurons: the role of calcium dynamics and IP3. *Biol Cybern* 82: 517–527, 2000.
- GLASS L AND MACKEY MC (Editors). *From Clocks to Chaos: The Rhythms of Life*. Princeton, NJ: Princeton Univ. Press, 1988.
- GLASS L, SHRIER A, AND BÉLAIR J. Chaotic cardiac rhythms. In: *Chaos*, edited by Holden AV. Princeton, NJ: Princeton Univ. Press, 1986, p. 237–256.
- GOLOMB D, WANG XJ, AND RINZEL J. Synchronization properties of spindle oscillations in a thalamic reticular nucleus model. *J Neurophysiol* 72: 1109–1126, 1994.
- GOLOWASH J, MANOR Y, AND NADIM F. Recognition of slow processes in rhythmic networks. *Trends Neurosci* 22: 375–377, 1999.
- GRAUBARD K, RAPER JA, AND HARTLINE DK. Graded synaptic transmission between spiking neurons. *Proc Natl Acad Sci USA* 77: 3733–3735, 1980.
- GRAY CM, KÖNIG P, ENGEL AK, AND SINGER W. Oscillatory responses in cat visual cortex exhibit inter-columnar synchronization which reflects global stimulus properties. *Nature* 338: 334–337, 1989.
- HARRIS-WARRICK RM, MARDER E, SELVERSTON AI, AND MOULINS M (Editors). *Dynamic Biological Networks. The Stomatogastric Nervous System*. Cambridge, MA: MIT Press, 1992.
- HAYASHI H AND ISHIZUKA S. Chaotic responses of the hippocampal CA3 region to a mossy fiber stimulation in vitro. *Brain Res* 686: 194–206, 1995.
- HAYASHI H, ISHIZUKA S, OHTA M, AND HIRAKAWA K. Chaotic behavior in the Onchidium giant neuron under sinusoidal stimulation. *Phys Lett A* 88: 435–438, 1992.
- HINDMARSH JL AND ROSE RM. A model of neuronal bursting using three coupled first order differential equations. *Proc R Soc Lond B Biol Sci* 221: 87–102, 1984.
- HOOPER SL. Transduction of temporal patterns by single neurons. *Nature Neurosci* 1: 720–726, 1998.
- JOHNSON BR, PECK JH, AND HARRIS-WARRICK RM. Amine modulation of electrical coupling in the pyloric network of the lobster stomatogastric ganglion. *J Comp Physiol [A]* 172: 715–732, 1993.
- KAPLAN DT, CLAY JR, MANNING T, GLASS L, GUEVARA MR, AND SHRIER A. Subthreshold dynamics in periodically stimulated squid axons. *Physiol Rev Lett* 76: 4074–4077, 1996.
- MACLEOD K, BÄCKER A, AND LAURENT G. Who reads temporal information contained across synchronized and oscillatory spike trains? *Nature* 395: 693–698, 1998.
- MANOR Y, NADIM F, ABBOTT LF, AND MARDER E. Temporal dynamics of graded synaptic transmission in the lobster stomatogastric ganglion. *J Neurosci* 17: 5610–5621, 1997.
- MARDER E. Computational dynamics in rhythmic neural circuits. *Neuroscientist* 3: 295–302, 1997.
- MARDER E AND EISEN JS. Transmitter identification of pyloric neurons: electrically coupled neurons use different transmitters. *J Neurophysiol* 51: 1345–1361, 1984.
- MATSUGU M, DUFFIN J, AND POON C. Entrainment, instability, quasi-periodicity, and chaos in a compound neural oscillator. *J Comput Neurosci* 5: 35–51, 1998.
- MORRIS LG AND HOOPER SL. Muscle response to changing neuronal input in the lobster (*Panulirus interruptus*) stomatogastric system: spike number-versus spike frequency-dependent domains. *J Neurosci* 17: 5956–5971, 1997.
- MULLONEY B AND SELVERSTON AI. Organization of the stomatogastric ganglion in the lobster. I. Neurons driving the lateral teeth. *J Comp Physiol* 91: 1–32, 1974.
- PAULIN MG. Digital filters for firing rate estimation. *Biol Cybern* 66: 525–531, 1992.
- PINTO RD, VARONA P, VOLKOVSKII AR, SZÚCS A, ABARBANEL HDI, AND RABINOVICH MI. Synchronous behavior of two coupled electronic neurons. *Physiol Rev E* 62: 2644–2656, 2000.
- RABINOVICH MI, ABARBANEL HDI, HUERTA R, ELSON R, AND SELVERSTON AI. Self-regularization in neural systems: experimental and theoretical results. *IEEE Trans Circ Syst* 44: 997–1005, 1997.
- RICHARDS KS, MILLER WL, AND MARDER E. Maturation of lobster stomatogastric ganglion rhythmic activity. *J Neurophysiol* 82: 2006–2009, 1999.
- RICHMOND BJ, OPTICAN LM, PODELL M, AND SPITZER H. Temporal encoding of two-dimensional patterns by single units in primate inferior temporal cortex. I. Response characteristics. *J Neurophysiol* 57: 132–146, 1987.
- RUSSELL DF AND HARTLINE DK. Slow active potentials and bursting motor patterns in pyloric network of the lobster, *Panulirus interruptus*. *J Neurophysiol* 48: 914–937, 1982.

- SEGUNDO JP, SUGIHARA G, DIXON P, STIBER M, AND BERSIER LF. The spike trains of inhibited pacemaker neurons seen through the magnifying glass of nonlinear analyses. *Neuroscience* 87: 741–766, 1998.
- SELVERSTON AI AND MILLER JP. Mechanisms underlying pattern generation in lobster stomatogastric ganglion as determined by selective inactivation of identified neurons. I. Pyloric system. *J Neurophysiol* 44: 1102–1121, 1980.
- SELVERSTON AI AND MOULINS M (Editors). *The Crustacean Stomatogastric Nervous System*. Berlin: Springer-Verlag, 1987.
- STEIN PSG, GRILLNER S, SELVERSTON AI, AND STUART DG (Editors). *Neurons, Networks, and Motor Behavior*. Cambridge, MA: MIT Press, 1997.
- STIBER M, PAKDAMAN K, VIBERT J, BOUSSARD E, SEGUNDO JP, NOMURA T, SATO S, AND DOI S. Complex responses of living neurons to pacemaker inhibition: a comparison of dynamical models. *Biosystems* 40: 177–188, 1997.
- SZŰCS A. Applications of the spike density function in analysis of neuronal firing patterns. *J Neurosci Methods* 81: 159–167, 1998.
- SZŰCS A, VARONA P, VOLKOVSKII ALEXANDER R, ABARBANEL HDI, RABINOVICH MI, AND SELVERSTON AI. Interacting biological and electronic neurons generate realistic oscillatory rhythms. *Neuroreport* 11: 563–569, 2000.
- TOMITA K. Periodically forced nonlinear oscillators. In: *Chaos*, edited by Holden AV. Princeton, NJ: Princeton Univ. Press, 1986, p. 211–236.
- TURRIGIANO G, LEMASSON G, AND MARDER E. Selective regulation of current densities underlies spontaneous changes in the activity of cultured neurons. *J Neurosci* 15: 3640–3652, 1995.
- WANG Y, WANG ZD, AND WANG W. Dynamical behaviors of periodically forced Hindmarsh-Rose neural model: the role of excitability and ‘intrinsic’ stochastic resonance. *J Physiol Soc Jpn* 69: 276–283, 2000.